This article has been accepted for publication in a future issue of this journal, but has not been fully edited. Content may change prior to final publication. Citation information: DOI 10.1109/TVT.2015.2395818, IEEE Transactions on Vehicular Technology

A Low-Complexity Architecture for PAPR Reduction in OFDM Systems with Near-Optimal Performance

Sen-Hung Wang, *Member, IEEE,* Kuan-Chou Lee, *Student Member, IEEE,* and Chih-Peng Li, *Senior Member, IEEE*

***Abstract*—Selected mapping (SLM) schemes are widely used to reduce the peak-to-average power ratio (PAPR) in orthogonal frequency division multiplexing (OFDM) systems. Various time-domain approaches have been proposed for reducing the number of inverse fast Fourier transform (IFFT) operations required to generate the candidate signals in traditional SLM schemes. However, the resulting time-domain generated signals are somewhat correlated, and thus the PAPR reduction performance is seriously degraded. Accordingly, the present study proposes a novel PAPR reduction method in which frequency-domain phase rotation, cyclic shifting, complex conjugate, and sub-carrier reversal operations are all employed in order to increase the diversity of the candidate signals. Furthermore, to circumvent the multiple-IFFT problem, all of the frequency-domain operations are converted into time-domain equivalents. It is shown that the sub-carrier partitioning and re-assembling processes are key to realizing low-complexity time-domain equivalent operations. Moreover, it is shown theoretically and numerically that the computational complexity of the proposed scheme is significantly lower than that of the traditional SLM method and the PAPR reduction performance is within 0.001 dB of that of SLM. Overall, the results indicate that among all of the low-complexity architectures proposed in the literature, the method proposed in this study most closely approximates the PAPR reduction performance of the traditional SLM scheme.**

***Index Terms*—Orthogonal frequency division multiplexing (OFDM), peak-to-average power ratio (PAPR), selected mapping (SLM).**

I. Introduction

ORTHOGONAL frequency division multiplexing (OFDM) is one of the most promising techniques for achieving high-rate data transmissions due to its high spectral efficiency and inherent robustness toward multi-path channels. However, OFDM systems suffer a high peak-to-average power ratio (PAPR) of the transmitted signals, which causes significant in-band distortion and out-of-band radiation when the signals are passed through a nonlinear power amplifier.

The literature contains various proposals for PAPR reduction, including tone reservation (TR) [1]-[3], companding [4], tone injection (TI) [5], active constellation extension (ACE) [6] [7], interleaving [8] [9], partial transmit sequence (PTS) [10]-[12], and selected mapping (SLM) [13]-[16]. Of these techniques, SLM is the most commonly applied due to its distortionless nature. However, the computational complexity of the traditional SLM scheme is extremely high since it requires a bank of inverse fast Fourier transform (IFFT) operations.

To address the problem multiple IFFTs, several low-complexity SLM architectures have been proposed [14]-[16] in which the frequency-domain phase rotation operations are converted into time-domain equivalent operations. For example, in [14], the IFFT operations are replaced by conversion vectors obtained by taking the IFFT of the phase rotation vectors. Similarly, in [15], the conversion vectors are specified in the form of perfect sequences [17]. However, the practical usefulness of these time-domain approaches as an alternative to the traditional SLM method depends on the time-domain equivalent operations having a low computational complexity. As a result, only a limited selection of sequences can be applied. Furthermore, since the adopted sequences are not randomly generated, but are somewhat correlated due to the low-complexity requirement, the frequency-domain equivalent phase rotations are not truly random, and thus a substantial degradation of the PAPR reduction performance occurs [15].

It is worth noting that a low-complexity interleaving-based PAPR reduction scheme has been proposed in [18], where three frequency-domain operations, namely, frequency-domain cyclic shifting, complex conjugate, and sub-carrier reversal, are adopted to scramble the sub-carriers thus to increase the PAPR diversity of various candidate signals. To circumvent the multiple-IFFT problem, the frequency-domain operations are converted into time-domain equivalents. It is demonstrated that this scheme outperforms traditional interleaving-based PAPR reduction scheme. However, there is significant performance loss relative to that of the traditional SLM scheme. Therefore, scrambling the sub-carriers is inadequate to reach the optimal PAPR reduction performance.

This paper proposes a novel architecture for reducing PAPR in OFDM systems with a lower computational complexity than the traditional SLM scheme whilst maintaining an equivalent

This paper was presented in part at the IEEE International Conference on Communications, 9-13 June, 2013.

Sen-Hung Wang is with the Institute of Communications Engineering, National Sun Yat-Sen University, Kaohsiung, Taiwan.

Kuan-Chou Lee is with the Graduate Institute of Communication Engineering, National Taiwan University, Taipei, Taiwan.

Chih-Peng Li (Corresponding Author) is with both the Institute of Communications Engineering and the Department of Electrical Engineering, National Sun Yat-Sen University, Kaohsiung, Taiwan 804, Tel:+886-7-5252000#4480; Email: cpli@faculty.nsysu.edu.tw.

This article has been accepted for publication in a future issue of this journal, but has not been fully edited. Content may change prior to final publication. Citation information: DOI 10.1109/TVT.2015.2395818, IEEE Transactions on Vehicular Technology

PAPR reduction performance. In contrast to the traditional SLM scheme, in which only frequency-domain phase rotation is used to generate the candidate signals, the method proposed in this study also applies frequency-domain cyclic shifting, complex conjugate, and sub-carrier reversal operations in order to increase the diversity of the candidate signals. Furthermore, to avoid the multiple-IFFT problem inherent in the traditional SLM method, all four frequency-domain operations are converted into time-domain equivalents. Of course, the time-domain equivalent operations should have a low computational complexity, which is the main challenge and contribution of this study. It is shown that through a careful partitioning and re-assembling of the sub-carriers, a low-complexity architecture can be successfully achieved. The theoretical analysis results show that the computational complexity of the proposed scheme is substantially lower than that of the traditional SLM method. Furthermore, the PAPR reduction performance of the proposed method is within 0.001 dB of that of the SLM scheme.

The remainder of this paper is organized as follows. Section II briefly describes the system model. Section III introduces the proposed PAPR reduction architecture in the frequency domain. Section IV describes the conversion of the frequency-domain operations of the proposed architecture to low-complexity time-domain equivalents. Section V discusses the implementation of the proposed PAPR reduction scheme in the time domain. Section VI analyzes the computational complexity of the proposed method. Section VII presents and discusses the simulation results. Finally, Section VIII provides some brief concluding remarks.

II. System Models

Consider an OFDM system with N sub-carriers. Let the modulated symbols form an $N \times 1$ frequency-domain data vector $\mathbf{X} = [X[0], X[1], \ldots, X[N-1]]^T$, where $X[k]$ denotes the modulated symbol of the kth sub-carrier and $(\cdot)^T$ is the transpose operation. An N-point IFFT operation is then performed to generate the time-domain signal vector $\mathbf{x}$, where the nth element of $\mathbf{x}$ is given by

$$x[n] = \frac{1}{\sqrt{N}} \sum_{k=0}^{N-1} X[k] \cdot \exp\left\{\frac{j2\pi nk}{N}\right\}, \quad n = 0, 1 \ldots, N-1. \tag{1}$$

The PAPR of the discrete-time OFDM signal is defined as

$$\text{PAPR}(\mathbf{x}) = \frac{\max\limits_{0 \le n \le N-1} |x[n]|^2}{E\left[|x[n]|^2\right]}, \tag{2}$$

where $E[\cdot]$ denotes the expectation operation. For OFDM systems, the PAPR reduction performance is generally evaluated by means of the complementary cumulative distribution function (CCDF), which is defined as the probability that the PAPR of $\mathbf{x}$ exceeds a given clip level γ, i.e.,

$$\text{CCDF}_{\text{PAPR}(\mathbf{x})} = \Pr\left(\text{PAPR}(\mathbf{x}) > \gamma\right). \tag{3}$$

III. Proposed PAPR Reduction Scheme in Frequency Domain

This section describes the implementation of the proposed PAPR reduction scheme in the frequency domain. In the traditional SLM scheme, the candidate signals are generated using frequency-domain phase rotation only. By contrast, in the scheme proposed in the present study, the PAPR diversity of the candidate signals is increased by performing additional frequency-domain cyclic shifting, complex conjugate, and sub-carrier reversal operations.

Consider an OFDM system with N sub-carriers. Let the sub-carriers be partitioned into S sub-carrier sets Γ_s, $s = 0, 1, \ldots, S-1$, where each set contains $\frac{N}{S}$ sub-carriers, in which $\frac{N}{S}$ is assumed to be a positive integer. In general, three methods exist for partitioning the sub-carriers in OFDM systems, namely the localized partitioning method (LPM), the distributed partitioning method (DPM), and the hybrid partitioning method (HPM).

In LPM, each sub-carrier set consists of a number of adjacent and consecutive sub-carriers, i.e., $\Gamma_s = \{i + s \cdot \frac{N}{S} | i = 0, 1, \ldots, \frac{N}{S} - 1\}$, $s = 0, 1, \ldots, S-1$. Meanwhile, in DPM, each sub-carrier set consists of multiple interleaved sub-carriers of equal spacing, i.e., $\Gamma_s = \{s + i \cdot S | i = 0, 1, \ldots, \frac{N}{S} - 1\}$, $s = 0, 1, \ldots, S-1$. Finally, in HPM, the sub-carriers are partitioned into U localized sub-carrier sets, which are then further partitioned into V distributed sets. In one extreme, if we set $U = 1$, HPM becomes DPM. In the other extreme, if we set $V = 1$, HPM becomes LPM. Therefore, both LPM and DPM can be regarded as special cases of HPM. The total number of sub-carrier sets is therefore equal to $S = U \cdot V$, with the set indexes being denoted as $s = u \cdot V + v$, where $u = 0, 1, \ldots, U-1$ and $v = 0, 1, \ldots, V-1$. In other words, the sub-carrier indexes of a given set are given by $\Gamma_s = \{\frac{N}{U} \cdot \lfloor \frac{s}{V} \rfloor + (s)_V + i \cdot V | i = 0, 1, \ldots, \frac{N}{S} - 1\}$, where $\lfloor \cdot \rfloor$ and $(\cdot)_V$ denote the floor function and the modulo V operation, respectively.

Figure 1(a) illustrates the HPM partitioning method for an OFDM system with $N = 16$ sub-carriers, $U = 2$, and $V = 4$. As shown, the 16 sub-carriers are first partitioned into $U = 2$ localized sub-carrier sets, where the first set consists of sub-carriers $\{0, 1, \ldots, 7\}$ and the second set consists of sub-carriers $\{8, 9, \ldots, 15\}$. Each sub-carrier set is then further partitioned into $V = 4$ sets, with each set consisting of 2 interleaved sub-carriers with a sub-carrier spacing of 4. In other words, the system contains a total of 8 sub-carrier sets, where (for example) the $s = 0$ sub-carrier set consists of the 0th and 4th sub-carriers, and the $s = 5$ sub-carrier set consists of the 9th and 13th sub-carriers.

For each of the sub-carrier partitioning methods described above, the frequency-domain data of sub-carrier set Γ_s are expressed in the form of an $N \times 1$ vector $\mathbf{X}_s$, in which the kth element of $\mathbf{X}_s$, $k = 0, 1, \ldots, N-1$, is given by

$$X_s[k] = \begin{cases} X[k], & k \in \Gamma_s, \\ 0, & \text{otherwise.} \end{cases} \tag{4}$$

It should be noted that all of the frequency-domain operations

This article has been accepted for publication in a future issue of this journal, but has not been fully edited. Content may change prior to final publication. Citation information: DOI 10.1109/TVT.2015.2395818, IEEE Transactions on Vehicular Technology

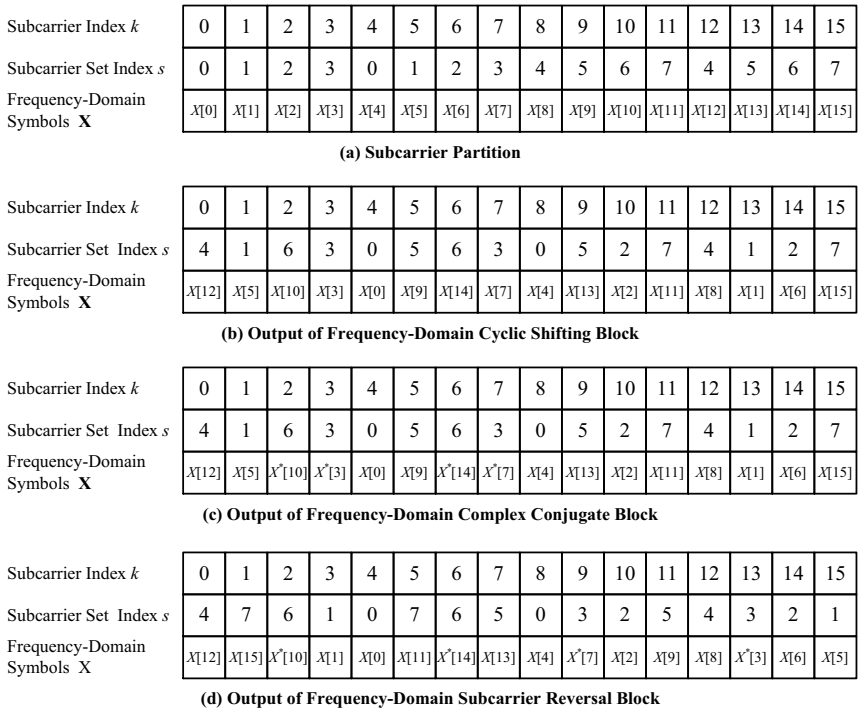

Fig. 1. Illustrative example of proposed scheme in frequency domain ($N = 16$, $U = 2$, $V = 4$).

described in the following are performed at the sub-carrier set level, i.e., $\mathbf{X}_s$.

Figure 2 presents a block diagram of the proposed PAPR reduction scheme in the frequency domain, where the frequency-domain data vector $\mathbf{X}$ is partitioned into S $N \times 1$ data vectors $\mathbf{X}_s$, $s = 0, 1, \ldots, S-1$. It is noted that in order to allow the maximum flexibility in partitioning the sub-carrier, the sub-carriers are partitioned using the HPM method. Note also that the kth element of $\mathbf{X}_s$ is given in (4) and the non-zero elements of $\mathbf{X}_s$ come from the modulated data symbols of sub-carrier set Γ_s. As shown in Fig. 2, the S data vectors $\mathbf{X}_s$, $s = 0, 1, \ldots, S-1$, are processed by multiple candidate signal generating blocks (CSGBs) in order to generate the candidate signals. (Note that each CSGB generates a single candidate signal.)

For illustration purposes, consider the mth CSGB in Fig. 2. The first block in the CSGB performs a frequency-domain cyclic shifting operation. Assuming that $l_{s,m}$ cyclic shifts are performed on $\mathbf{X}_s$, the output signal is denoted as $\mathbf{A}_{s,m}$, $s = 0, 1, \ldots, S-1$, $m = 1, 2, \ldots, M$. Therefore, the kth element of $\mathbf{A}_{s,m}$ is given by

$$A_{s,m}[k] = X_s[(k - l_{s,m})_N], \ k = 0, 1, \ldots, N-1, \qquad (5)$$

where $(\cdot)_N$ denotes the modulo N operation. Consider Fig. 1(a) and take the $s = 0$ sub-carrier set with $l_{0,m} = 4$ for illustration purposes. For the $s = 0$ sub-carrier set, consisting of the 0th and 4th sub-carriers, the corresponding data symbols, $X[0]$ and $X[4]$, are cyclically shifted to the 4th and 8th sub-carriers, respectively (see Fig. 1(b)). Similarly, for the $s = 5$ sub-carrier set with $l_{5,m} = 12$, the corresponding data symbols, $X[9]$ and $X[13]$, are cyclically shifted to the 5th and 9th sub-carriers, respectively. Note that the selection of the cyclic shift value $l_{s,m}$ for a given m is not arbitrary, but is jointly considered over various s since different sub-carrier sets cannot occupy the same sub-carrier after the cyclic shifting operation. For example, $[l_{0,m}\ l_{1,m}\ \cdots\ l_{7,m}] = [4\ 12\ 8\ 0\ 4\ 12\ 8\ 0]$ is an acceptable combination of cyclic shifts since the sub-carriers of the different sub-carrier sets do not overlap one another following shifting, as shown in Fig. 1(b).

The second block of the CSGB performs frequency-domain phase rotation. The output of the sth sub-carrier set for the mth CSGB is denoted as $\mathbf{B}_{s,m}$, with the kth element being given by

$$B_{s,m}[k] = \theta_{s,m}[k] \cdot A_{s,m}[k], \ k = 0, 1, \ldots, N-1, \qquad (6)$$

where $\theta_{s,m}[k]$ is a complex number with a unit magnitude. (Note that the phase rotation operation is omitted from Fig. 1 for the sake of simplicity.)

The third block of the CSGB performs a frequency-domain conjugate operation and yields an output signal $\mathbf{C}_{s,m}$. In order to generate multiple candidate signals with an uncorrelated PAPR, each sub-carrier set arbitrarily chooses whether or not to perform the conjugate operation, i.e., $C_{s,m}[k] = B_{s,m}[k]$ or $C_{s,m}[k] = B^*_{s,m}[k]$, $\forall k \in \Gamma_s$, where * denotes the complex conjugate operation. Consider the example shown in Fig. 1(b). Assume that the conjugate operation is performed only on sub-carrier sets $s = 3$ (i.e., the 3rd sub-carrier with $X[3]$ and the 7th sub-carrier with $X[7]$) and $s = 6$ (i.e., the 2nd sub-carrier with $X[10]$ and the 6th sub-carrier with $X[14]$). The corresponding output signals are shown in Fig. 1(c), in which a total of four conjugate operations are performed.

The fourth block of the CSGB performs a frequency-domain sub-carrier reversal operation on the sub-carrier sets, i.e., $F_{s,m}[k] = C_{s,m}[(-k)_N], \ \forall k \in \Gamma_s$. Notably, as for the

This article has been accepted for publication in a future issue of this journal, but has not been fully edited. Content may change prior to final publication. Citation information: DOI 10.1109/TVT.2015.2395818, IEEE Transactions on Vehicular Technology

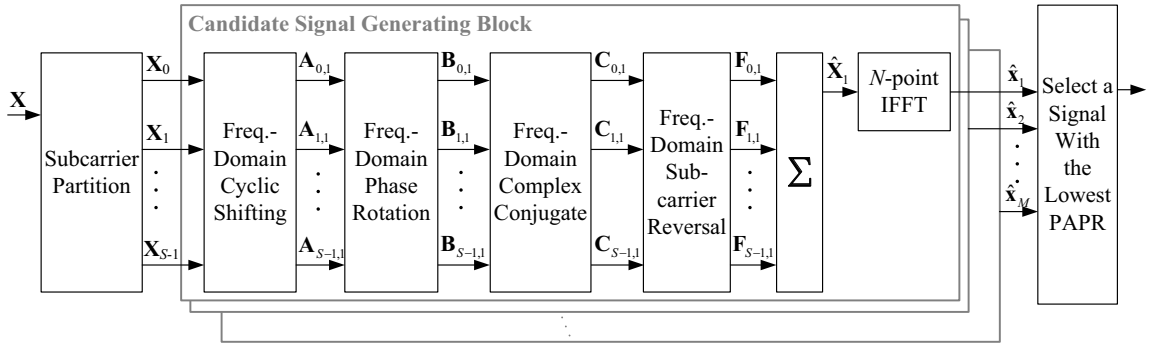

Fig. 2. System architecture of proposed scheme in frequency domain.

conjugate operation, each sub-carrier set may or may not choose to perform sub-carrier reversal. However, in this case, the choice of whether or not to perform the reversal operation is not arbitrary, but is jointly considered since different sub-carrier sets cannot occupy the same sub-carriers after the sub-carrier reversal process. For example, if the sub-carrier reversal operation is performed on sub-carrier sets $s = 1, 3, 5$ and 7 in Fig. 1(c), but sub-carrier sets $s = 0, 2, 4$ and 6 remain unchanged, the output signals have the form shown in Fig. 1(d), where (for example) the $s = 7$ sub-carrier set is moved from sub-carriers $k = 15$ $(X[15])$ and $k = 11$ $(X[11])$ to sub-carriers $k = 1$ $(X[15])$ and $k = 5$ $(X[11])$, respectively.

Finally, the mth candidate signal in the frequency domain is obtained by summing up the various sub-carrier sets of the corresponding CSGB, i.e.,

$$\hat{\mathbf{X}}_m = \sum_{s=0}^{S-1} \mathbf{F}_{s,m}. \tag{7}$$

The candidate signal in the time domain, i.e., $\hat{\mathbf{x}}_m$ is obtained by performing an IFFT operation on $\hat{\mathbf{X}}_m$. Having generated M candidate signals, the signal with the lowest PAPR is selected for transmission.

The scheme described above requires M IFFT operations since all of the operations are performed in the frequency domain and each candidate signal requires its own IFFT. As a result, the computational complexity of the proposed scheme is extremely high. In theory, this problem can be avoided by converting the four frequency-domain operations described above into time-domain equivalents. However, this conversion process cannot be performed by simply taking the corresponding IFFT since the time-domain operations should also have a low computational complexity. Thus, in the following section, a more computationally-efficient approach is proposed.

IV. Time-Domain Signal Properties of OFDM Systems

In this section, the complexity of the frequency-domain architecture described above is reduced by means of four time-domain equivalent properties. In addition, a time-domain repetition property is introduced in order to further reduce the computational complexity. Note that all of the operations described in this section (both frequency-domain and time-domain) are performed on the sub-carriers of the same set.

Property 1: Frequency-Domain Cyclic Shifting / Time-Domain Phase Rotation

Performing cyclic shifting on the frequency-domain data vector $\mathbf{X}$ is equivalent to performing phase rotation on the corresponding time-domain data vector $\mathbf{x}$, i.e.,

$$\mathcal{F}^{-1}\left\{X[(k-l)_N]\right\} = x[n]\cdot \exp\left\{\frac{j2\pi nl}{N}\right\}, \quad l = 0, 1, \ldots, N-1, \tag{8}$$

where $\mathcal{F}^{-1}\{\cdot\}$ denotes the IFFT operation, and l is the number of frequency-domain cyclic shifts. Note that for $l \in \{0, \frac{N}{4}, \frac{N}{2}, \frac{3N}{4}\}$, we have $\exp\{j2\pi nl/N\} \in \{\pm 1, \pm j\}$ and the time-domain equivalent operation on the right hand side of (8) does not require any complex multiplications or additions. Note also that the choice of cyclic shifts l is not arbitrary, but is jointly considered over multiple sub-carrier sets since different sub-carrier sets must not occupy the same sub-carriers following the frequency-domain cyclic shifting operation.

Property 2: Frequency-Domain Phase Rotation / Time-Domain Cyclic Shifting

Performing phase rotation on the frequency-domain data vector $\mathbf{X}$ is equivalent to performing cyclic shifting on the corresponding time-domain data vector $\mathbf{x}$, i.e.,

$$\mathcal{F}^{-1}\left\{X[k]\cdot \exp\left\{\frac{-j2\pi kw}{N}\right\}\right\} = x[(n-w)_N], \quad w = 0, 1, \ldots, N-1, \tag{9}$$

where w is the number of time-domain cyclic shifts. It is seen that the time-domain equivalent operation on the right hand side of (9) does not require any complex multiplications or additions.

Property 3: Frequency-Domain Complex Conjugate / Time-Domain Complex Conjugate of Time-Reversed Signals

Performing the frequency-domain complex conjugate operation is equivalent to performing the complex conjugate operation on the time-reversed signals, i.e.,

$$\mathcal{F}^{-1}\left\{X^*[k]\right\} = x^*[(-n)_N]. \tag{10}$$

Property 4: Frequency-Domain Sub-carrier Reversal / Time-Domain Signal Reversal

This article has been accepted for publication in a future issue of this journal, but has not been fully edited. Content may change prior to final publication. Citation information: DOI 10.1109/TVT.2015.2395818, IEEE Transactions on Vehicular Technology

Performing sub-carrier reversal on the frequency-domain data vector $\mathbf{X}$ is equivalent to performing time-domain reversal operation on data vector $\mathbf{x}$, i.e.,

$$\mathcal{F}^{-1}\{X[(-k)_N]\} = x[(-n)_N]. \quad (11)$$

It should be noted that the frequency-domain sub-carrier reversal operation cannot be performed on arbitrary sub-carrier sets since this may result in different sub-carrier sets occupying the same sub-carriers. Thus, a number of remarks are given in the following to clarify the applicability of the subcarrier reversal operation for the three sub-carrier partitioning methods.

Remark 1: For the case of the LPM partitioning method, performing the frequency-domain sub-carrier reversal operation on a given sub-carrier set will in general cause sub-carrier overlapping with another set of sub-carriers. Therefore, the frequency-domain sub-carrier reversal operation cannot be performed when using the LPM scheme.

Remark 2: For the case of DPM, sub-carrier reversal can be performed on either Γ_0 or $\Gamma_{S/2}$ individually since different sub-carrier sets will not occupy the same sub-carriers after the frequency-domain sub-carrier reversal process. However, sub-carrier reversal cannot be performed on sub-carrier sets $\Gamma_{s'}$, $s' = 1, 2, \ldots, \frac{S}{2} - 1$ individually. Nevertheless, sub-carrier reversal can be performed on $\Gamma_{s'}$ and $\Gamma_{S-s'}$ simultaneously without causing sub-carrier overlapping.

Consider an OFDM system with 16 sub-carriers, where each sub-carrier is partitioned into $S = 4$ DPM sub-carrier sets, i.e., $\Gamma_0 = \{0, 4, 8, 12\}$, $\Gamma_1 = \{1, 5, 9, 13\}$, $\Gamma_2 = \{2, 6, 10, 14\}$ and $\Gamma_3 = \{3, 7, 11, 15\}$. Take sub-carrier set Γ_0 for illustration purposes. Assuming that the frequency-domain sub-carrier reversal operation is performed, the corresponding sub-carriers become $\Gamma_0 = \{0, 12, 8, 4\}$. It can be seen that the sub-carriers still belong to the same sub-carrier set and different sub-carrier sets do not occupy the same sub-carriers. Notably, if the frequency-domain sub-carrier reversal operation is performed only on Γ_1, the resulting sub-carriers become $\{15, 11, 7, 3\}$, and therefore occupy the same sub-carriers as sub-carrier set $\Gamma_3 = \{3, 7, 11, 15\}$. However, if the frequency-domain sub-carrier reversal operation is performed on both Γ_1 and Γ_3 simultaneously, the resulting sub-carriers become $\{15, 11, 7, 3\}$ and $\{13, 9, 5, 1\}$, respectively. In other words, different sub-carrier sets do not occupy the same sub-carriers.

Remark 3: For the HPM partitioning method, performing the frequency-domain sub-carrier reversal operation on a given sub-carrier set will inevitably cause sub-carrier overlapping with another set of sub-carriers. However, if different sets of sub-carriers are properly re-assembled such that the partitioning among them is equivalent to that obtained using DPM, the frequency-domain sub-carrier reversal operation can be adopted in the same way as that described in *Remark 2*.

Consider the OFDM system shown in Fig. 1(a) with $N = 16$, $U = 2$ and $V = 4$. If frequency-domain sub-carrier reversal is performed on $\Gamma_1 = \{1, 5\}$, the resulting sub-carrier set occupies sub-carriers $\{15, 11\}$, i.e., the sub-carriers overlap those in sub-carrier set Γ_7. However, if the sub-carrier sets are properly re-assembled, e.g., $\bar{\Gamma}_{\bar{s}=0} \equiv \Gamma_0 \cup \Gamma_4 = \{0, 4, 8, 12\}$, $\bar{\Gamma}_{\bar{s}=1} \equiv \Gamma_1 \cup \Gamma_5 = \{1, 5, 9, 13\}$, $\bar{\Gamma}_{\bar{s}=2} \equiv \Gamma_2 \cup \Gamma_6 = \{2, 6, 10, 14\}$, and $\bar{\Gamma}_{\bar{s}=3} \equiv \Gamma_3 \cup \Gamma_7 = \{3, 7, 11, 15\}$, the partition is converted into the form of $V = 4$ DPM sub-carrier sets. Therefore, the frequency-domain sub-carrier reversal operation can be performed on each of these four re-assembled sub-carrier sets in the same way as that described in *Remark 2*.

Property 5: Time-Domain Repetition

In DPM, the frequency-domain sub-carriers of any set Γ_s have an equal spacing S. Consequently, the time-domain signal vector $\mathbf{x}_s$ has the following repetition characteristic [16]:

$$\mathbf{x}_s = \left[\mathbf{x}_s^{(0)} \quad \beta_{s,1}\mathbf{x}_s^{(0)} \quad \beta_{s,2}\mathbf{x}_s^{(0)} \quad \cdots \quad \beta_{s,S-1}\mathbf{x}_s^{(0)}\right]^T, \quad (12)$$

where $\mathbf{x}_s^{(0)}$ is a $1 \times \frac{N}{S}$ vector consisting of the first $\frac{N}{S}$ elements of $\mathbf{x}_s$, $\beta_{s,i} = \exp\{j2\pi i \cdot s/S\}$, $i = 1, 2, \ldots, S-1$. It is noted that $\beta_{s,i} \in \{\pm 1, \pm j\}$ when $S = 2, 4$.

Furthermore, in HPM, the sub-carriers have an equal spacing of V. Thus, the following property can be obtained:

$$\mathbf{x}_s = \left[\mathbf{x}_s^{(0)} \quad \beta_{s,1}\mathbf{x}_s^{(0)} \quad \beta_{s,2}\mathbf{x}_s^{(0)} \quad \cdots \quad \beta_{s,V-1}\mathbf{x}_s^{(0)}\right]^T, \quad (13)$$

where $\mathbf{x}_s^{(0)}$ is a $1 \times \frac{N}{V}$ vector consisting of the first $\frac{N}{V}$ elements of $\mathbf{x}_s$, $\beta_{s,i'} = \exp\{j2\pi i' \cdot s/V\}$, $i' = 1, 2, \ldots, V-1$. It is noted that $\beta_{s,i'} \in \{\pm 1, \pm j\}$ when $V = 2, 4$.

V. The Proposed Low-Complexity PAPR Reduction Scheme in the Time Domain

Section III has described the implementation of the proposed PAPR reduction scheme in the frequency-domain. However, as discussed, each candidate signal requires the use of an N-point IFFT operation, and thus the scheme has a high computational complexity. To resolve this problem, this section utilizes the time-domain equivalent operations derived in Section IV to construct a low-complexity architecture for PAPR reduction.

Figure 3 presents a block diagram of the proposed architecture, in which the frequency-domain data vector $\mathbf{X}$ is partitioned into S data vectors $\mathbf{X}_s$ of size $N \times 1$, $s = 0, 1, \ldots, S-1$, in accordance with (4). Note that in implementing the proposed architecture, the HPM sub-carrier partitioning method is adopted in order to maximize the PAPR diversity. As shown in Fig. 3, having partitioned the sub-carriers, an IFFT operation is performed on $\mathbf{X}_s$ to obtain the corresponding time-domain data vector $\mathbf{x}_s$ of size $N \times 1$. It is noted that although the proposed scheme still requires S N-point IFFT operations, the computational complexity of the proposed architecture is much lower than that of the traditional SLM scheme since S ($S = 2$ or 4 in this study) is much smaller than the number of candidate signals M. Furthermore, the computational complexity of each N-point IFFT is significantly decreased in the proposed scheme since most of the elements of $\mathbf{X}_s$ are zero [19]. (Note that a detailed complexity analysis of the propose architecture is presented in Section VI.)

Following the IFFT operations, the time-domain data vectors $\mathbf{x}_s$, $s = 0, 1, \ldots, S-1$, are processed by M CSGBs in order to generate M candidate signals. It is noted that the summation of $\mathbf{x}_s$ generates the original time-domain transmitted signal. In each of the M CSGBs, each $\mathbf{x}_s$ is first processed by the time-domain phase rotation block (i.e., the time-domain

This article has been accepted for publication in a future issue of this journal, but has not been fully edited. Content may change prior to final publication. Citation information: DOI 10.1109/TVT.2015.2395818, IEEE Transactions on Vehicular Technology

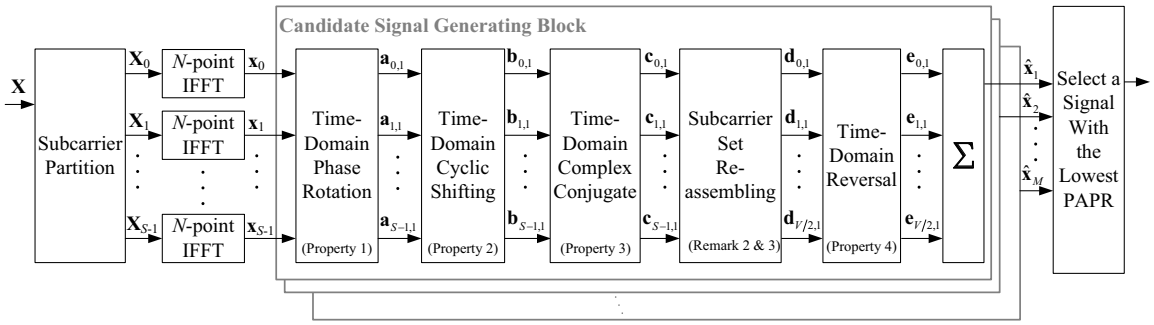

Fig. 3. System architecture of proposed scheme in time domain.

equivalent of the frequency-domain cyclic shifting operation). The resulting output signal is denoted as $\mathbf{a}_{s,m}$, where the nth element is given by

$$a_{s,m}[n] = x_s[n] \cdot \exp\left\{\frac{j2\pi n \cdot l_{s,m}}{N}\right\}, \quad n = 0, 1, \ldots, N-1, \tag{14}$$

in which $x_s[n]$ is the nth element of $\mathbf{x}_s$ and $l_{s,m}$ is the number of frequency-domain cyclic shifts of Γ_s for the mth candidate signal. As explained in Section III (*Property 1*), the selection of the cyclic shift value $l_{s,m}$ for a given m is not arbitrary, but is based on a joint consideration over various s. *Property 1* also provide the cases of $l_{s,m}$ that result in a low computational complexity.

The second block of the CSGB performs a time-domain cyclic shifting operation, i.e., the time-domain equivalent of the frequency-domain phase rotation operation. Therefore, the nth element of the output signal $\mathbf{b}_{s,m}$ has the form

$$b_{s,m}[n] = a_s[(n - w_{s,m})_N], \ n = 0, 1, \ldots, N-1, \tag{15}$$

where $w_{s,m}$ denotes the number of cyclic shifts of the sth sub-carrier set for the mth CSGB. It will be recalled that the frequency-domain phase rotation operation is not arbitrary, but is governed by (9). In practice, phase rotation is not completely random, and thus the PAPR reduction performance is slightly degraded. However, this drawback is minor compared to the substantial reduction achieved in the computational complexity of the proposed scheme.

The third block in Fig. 3 performs the time-domain complex conjugate operation, i.e., the equivalent operation of the frequency-domain complex conjugate process. Since the system arbitrarily chooses whether or not to perform the complex conjugate operation, the nth element of the output signal $\mathbf{c}_{s,m}$ has the form

$$c_{s,m}[n] = b_{s,m}[n] \quad \text{or} \quad b^*_{s,m}[(-n)_N]. \tag{16}$$

As discussed in Section III (*Property 4*), the sub-carrier sets must be properly re-assembled before performing the time-domain signal reversal operation. In particular, when using the HPM partitioning method, the sub-carrier sets must be reassembled in such a way that the partition is equivalent to that obtained using DPM (*Remark 3*). Furthermore, for the case of DPM, the time-domain signal reversal operation can be applied on either $\Gamma_{s=0}$ or $\Gamma_{s=S/2}$ individually, but should be performed on Γ_s and Γ_{S-s} simultaneously, $s = 1, 2, \ldots, \frac{S}{2} - 1$, in order to avoid sub-carrier overlaps (*Remark 2*). Therefore, the fourth block of the time-domain CSGB performs a sub-carrier set re-assembling function, which consists of the two steps shown in Fig. 4. In the first step, the S HPM sub-carrier sets Γ_s, $s = 0, 1, \ldots, S-1$ $(S = U \cdot V)$, are combined to obtain V DPM sub-carrier sets $\bar{\Gamma}_{\bar{s}}$, $\bar{s} = 0, 1, \ldots, V-1$. As shown in Fig. 4, the $\bar{s}$th DPM sub-carrier set is obtained by combining the outputs of time-domain complex conjugate operations $\mathbf{c}_{(u \cdot V + \bar{s}),m}$, $u = 0, 1, \ldots, U-1$, i.e.,

$$\bar{\mathbf{c}}_{\bar{s},m} = \sum_{u=0}^{U-1} \mathbf{c}_{(u \cdot V + \bar{s}),m}, \ \bar{s} = 0, 1, \ldots, V-1. \tag{17}$$

In the second step, sub-carrier sets $\bar{\Gamma}_{\bar{s}}$ and $\bar{\Gamma}_{S-\bar{s}}$, $\bar{s} = 1, 2, \ldots, \frac{V}{2} - 1$, are combined to form a single sub-carrier set $\breve{\Gamma}_q$, $q = 1, 2, \ldots, \frac{V}{2} - 1$, while leaving $\bar{\Gamma}_{\bar{s}=0}$ and $\bar{\Gamma}_{\bar{s}=V/2}$ unchanged, i.e.,

$$\mathbf{d}_{q,m} = \begin{cases} \bar{\mathbf{c}}_{0,m}, & q = 0, \\ \bar{\mathbf{c}}_{\frac{V}{2},m}, & q = \frac{V}{2}, \\ \bar{\mathbf{c}}_{q,m} + \bar{\mathbf{c}}_{V-q,m}, & q = 1, 2, \ldots, \frac{V}{2} - 1. \end{cases} \tag{18}$$

Substituting (17) into (18) yields

$$\mathbf{d}_{q,m} = \begin{cases} \sum_{u=0}^{U-1} \mathbf{c}_{u \cdot V,m}, & q = 0, \\ \sum_{u=0}^{U-1} \mathbf{c}_{u \cdot V + \frac{V}{2},m}, & q = \frac{V}{2}, \\ \sum_{u=0}^{U-1} \mathbf{c}_{u \cdot V + q,m} + \sum_{u=0}^{U-1} \mathbf{c}_{u \cdot V + (V-q),m}, & q = 1, 2, \ldots, \frac{V}{2} - 1. \end{cases} \tag{19}$$

It is worth noting that all operations before re-assembling are performed by HPM. Thus, the resulting signals are not equivalent to those obtained by DPM from the beginning.

It is noted that the Sub-carrier Set Re-assembling block of the proposed time-domain architecture uses the time-domain repetition property (i.e., *Property 5*) in order to reduce the computational complexity. Thus, as shown in Fig. 4, in the first step, it is necessary only to generate the first N/V

This article has been accepted for publication in a future issue of this journal, but has not been fully edited. Content may change prior to final publication. Citation information: DOI 10.1109/TVT.2015.2395818, IEEE Transactions on Vehicular Technology

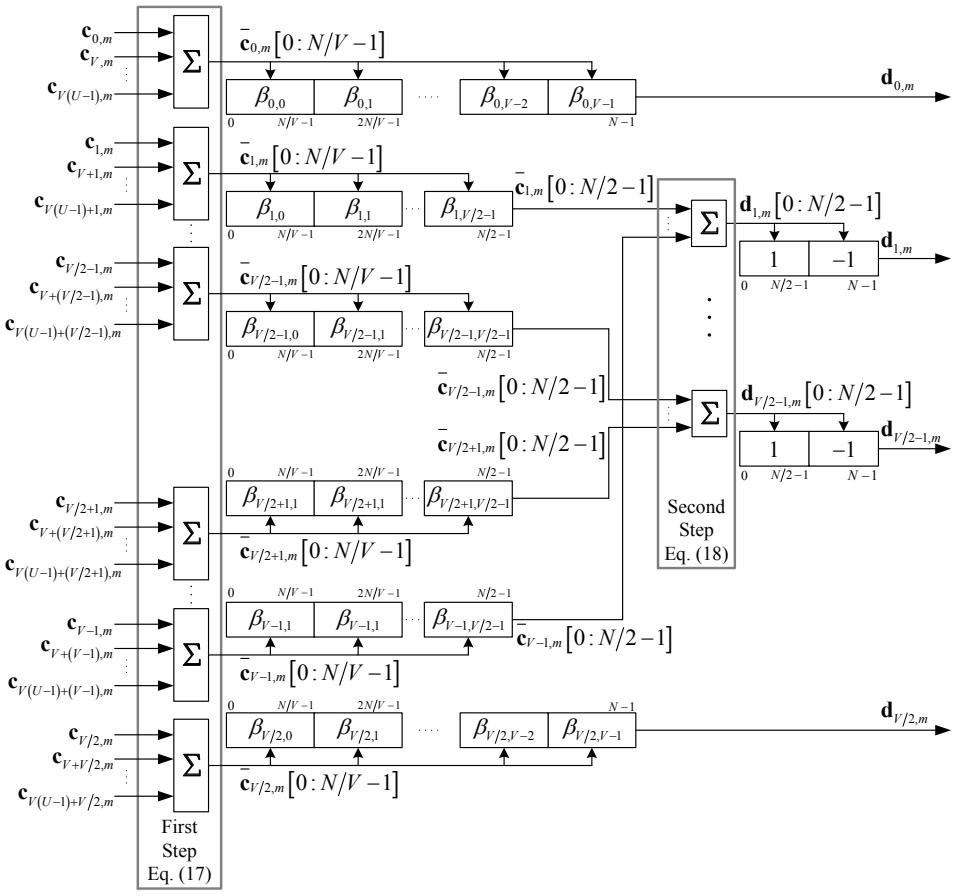

Fig. 4. Details of Sub-carrier Set Re-assembling operation.

elements of $\bar{\mathbf{c}}_{\bar{s},m}$, $\bar{s} = 0, 1, \ldots, V-1$. In other words, the remaining $N - N/V$ elements of $\bar{\mathbf{c}}_{0,m}$ and $\bar{\mathbf{c}}_{V/2,m}$ can be obtained directly using *Property 5*. Similarly, for $\bar{\mathbf{c}}_{\bar{s},m}$, $\bar{s} = 1, 2, \ldots, V/2-1, V/2+1, \ldots, V-1$, only the first $N/2$ elements are obtained from the first N/V elements using the time-domain repetition property and are sent to the second stage. In the second step, the first $N/2$ elements of $\bar{\mathbf{c}}_{q,m} + \bar{\mathbf{c}}_{V-q,m}$, $q = 1, 2, \ldots, \frac{V}{2} - 1$ are obtained and the remaining $N/2$ elements are then generated using the time-domain repetition property once again. It is worth noting that applying the time-domain repetition property does not involve any complex multiplications when $V = 2, 4$ since $\beta_{\bar{s},i} \in \{\pm 1, \pm j\}$.

Figure 5 presents an illustrative example of the re-assembling operation for the case of eight time-domain signals, $\mathbf{c}_{s,m}$, $s = 0, 1, \ldots, 7$, corresponding to the eight frequency-domain sub-carrier sets shown in Fig. 1(c). The sub-carrier sets are firstly re-assembled such that the partition is converted from a HPM form to a DPM form, i.e., $\bar{\Gamma}_{\bar{s}=0} = \Gamma_0 \cup \Gamma_4 = \{0, 4, 8, 12\}$, $\bar{\Gamma}_{\bar{s}=1} = \Gamma_1 \cup \Gamma_5 = \{1, 5, 9, 13\}$, $\bar{\Gamma}_{\bar{s}=2} = \Gamma_2 \cup \Gamma_6 = \{2, 6, 10, 14\}$ and $\bar{\Gamma}_{\bar{s}=3} = \Gamma_3 \cup \Gamma_7 = \{3, 7, 11, 15\}$, resulting in $V = 4$ DPM sub-carrier sets. Sub-carrier sets $\bar{\Gamma}_1$ and $\bar{\Gamma}_3$ are then combined to form a single sub-carrier set $\breve{\Gamma}_1$. In addition, we have $\breve{\Gamma}_0 = \bar{\Gamma}_0$ and $\breve{\Gamma}_2 = \bar{\Gamma}_2$. Therefore, the output of the re-assembling operation comprises three signals, namely $\mathbf{d}_{q,m}$, $q = 0, 1$ and 2, as given in (19).

The sub-carrier set re-assembling operation is followed by the time-domain signal reversal process (see Fig. 3). As with the complex conjugate operation, the system arbitrarily chooses whether or not to perform the reversal operation. The nth element of the resulting signal $\mathbf{e}_{q,m}$, $q = 0, 1, \ldots, \frac{V}{2}$, therefore has the form

$$e_{q,m}[n] = d_{q,m}[n] \quad \text{or} \quad d_{q,m}[(-n)_N], \; q = 0, 1, \ldots, \frac{V}{2}. \tag{20}$$

Finally, the mth candidate signal is obtained by adding all the $\mathbf{e}_{q,m}$ of the mth CSGB, to give

$$\hat{\mathbf{x}}_m = \sum_{q=0}^{V/2} \mathbf{e}_{q,m}. \tag{21}$$

Having generated M candidate signals, the signal with the lowest PAPR is selected for transmission. It should be noted that the proposed scheme requires various operations at the transmitter, but the related parameters can be stored at both the transmitter and receiver with code book. Therefore, the number of side information bits depends only on the number of candidate signals. If M candidate signals are generated, the scheme requires only $\log_2\lceil M \rceil$ bits to transmit side information. In addition, the side information is assumed to be transmitted through the control channel, where channel coding is adopted to protect the side information from being erroneously detected.

This article has been accepted for publication in a future issue of this journal, but has not been fully edited. Content may change prior to final publication. Citation information: DOI 10.1109/TVT.2015.2395818, IEEE Transactions on Vehicular Technology

Subcarrier Index k	0	1	2	3	4	5	6	7	8	9	10	11	12	13	14	15
Subcarrier Set Index s	4	1	6	3	0	5	6	3	0	5	2	7	4	1	2	7
Combined Subcarrier Set Index $\bar{s}$	0	1	2	3	0	1	2	3	0	1	2	3	0	1	2	3
Index q in (19)	0	1	2	1	0	1	2	1	0	1	2	1	0	1	2	1
Frequency-Domain Symbols $\mathbf{X}$	$X[12]$	$X[5]$	$X^*[10]$	$X^*[3]$	$X[0]$	$X[9]$	$X^*[14]$	$X^*[7]$	$X[4]$	$X[13]$	$X[2]$	$X[11]$	$X[8]$	$X[1]$	$X[6]$	$X[15]$

Fig. 5. Illustrative example of Sub-carrier Set Re-assembling operation ($N = 16$, $U = 2$, $V = 4$).

VI. Analysis of Computational Complexity

This section evaluates the computational complexities of the traditional SLM scheme and the proposed PAPR reduction scheme, respectively. As described in Section III, the traditional SLM scheme requires M N-point IFFTs to generate M different candidate signals, where each N-point IFFT requires $\frac{N}{2} \cdot \log_2 N$ complex multiplications and $N \cdot \log_2 N$ complex additions. Therefore, the total number of complex multiplications and complex additions are $\frac{MN}{2} \cdot \log_2 N$ and $MN \cdot \log_2 N$, respectively.

For the PAPR reduction scheme proposed in this study, a total of S N-point IFFTs and M CSGBs are required to generate M candidate signals. As described in Section III, the HPM partitioning method is adopted in order to maximize the PAPR diversity. Therefore, the sub-carriers are partitioned into $S = U \cdot V$ sets. In the proposed architecture, most elements of the inputs to the IFFTs, i.e., $\mathbf{X}_s$ in (4), are zeros, and thus the IFFTs can be readily computed using the efficient algorithm proposed in [19]. It can be shown that the total number of complex multiplications and complex additions for S IFFT operations is therefore equal to $\frac{UN}{2} \cdot \log_2(\frac{N}{U \cdot V}) + N \cdot (U-1)$ and $UN \cdot \log_2(\frac{N}{U \cdot V})$, respectively.

Regarding the computational complexity of each CSGB, *Property 1* demonstrates that the time-domain equivalent operation on the right hand side of (8) does not require any complex multiplications or additions when the number of frequency-domain cyclic shifts belongs to $\{0, \frac{N}{4}, \frac{N}{2}, \frac{3N}{4}\}$, which implies that $U = 2$ or $U = 4$ should be adopted. Furthermore, *Property 5* indicates that $V = 2, 4$ yields a significant reduction in the computational complexity. Therefore, four different combinations of U and V are considered in the remainder of this study, i.e., $(U, V) \in \{(2,2),\ (2,4),\ (4,2),\ (4,4)\}$. However, increasing U and V increases the complexity of the PAPR reduction process. Furthermore, a series of preliminary simulations showed that there was no significant change in the PAPR reduction performance of the proposed scheme when using higher values of U and V. Thus, in evaluating the performance of the proposed scheme, higher values of U and V were not considered.

Since $U = 2, 4$ and $V = 2, 4$ were adopted, the first three blocks of the CSGBs in the proposed scheme, i.e., the time-domain phase rotation, time-domain cyclic shifting, and time-domain complex conjugate operations, do not require any complex multiplications or additions, as indicated in *Property 1*, *2*, and *3*.

Regarding the Sub-carrier Set Re-assembling process, for the case of $V = 2$, only the first two terms in (19), i.e., $\sum_{u=0}^{U-1} \mathbf{c}_{2u,m}$ and $\sum_{u=0}^{U-1} \mathbf{c}_{2u+1,m}$, need be considered since the third term does not exist. Furthermore, the number of complex additions can be reduced using the time-domain repetition property (i.e., *Property 5*). In other words, only the first $\frac{N}{V} = \frac{N}{2}$ elements of $\mathbf{d}_{0,m}$ and $\mathbf{d}_{1,m}$ need be generated, requiring a total of $2 \cdot (U-1) \cdot \frac{N}{V}$ complex additions. For the case of $V = 4$, the first two terms, $\mathbf{d}_{0,m}$ and $\mathbf{d}_{2,m}$, require $2 \cdot (U-1) \cdot \frac{N}{V}$ complex additions. For the third term in (19), the summations in the first and second steps of the sub-carrier set re-assembling operations require $(V-2) \cdot (U-1) \cdot \frac{N}{V}$ and $\frac{V-2}{2} \cdot \frac{N}{2}$ complex additions, respectively. Thus, the sub-carrier set re-assembling operation requires a total of $(U-1) \cdot N + \frac{(V-2) \cdot N}{4}$ complex additions for both $V = 2$ and $V = 4$, and no complex multiplications.

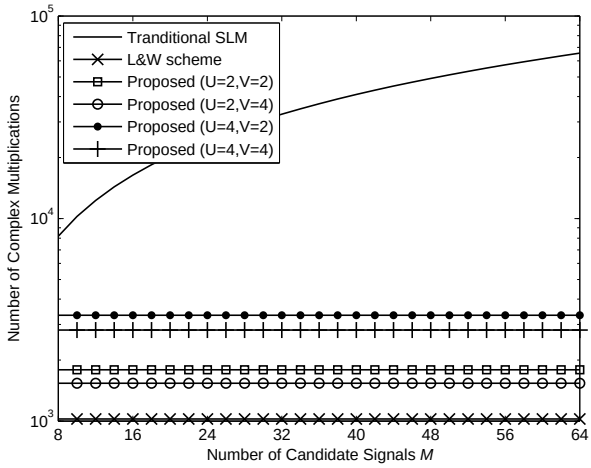

Fig. 6. Number of complex multiplications as function of number of candidate signals M ($N = 256$).

The fourth block in the CSGB performs the time-domain signal reversal operation. As shown in (20), the reversal operation requires neither complex multiplications nor complex additions. The final step of the CSGB generates the candidate signal by summing up the various signal components, as shown in (21). For the case of $V = 2$, $\mathbf{e}_{0,m}$ is directly added to $\mathbf{e}_{V/2,m}$. For the case of $V = 4$, in accordance with the repetition property shown in *Property 5*, $\mathbf{e}_{0,m}$ and $\mathbf{e}_{V/2,m}$ are added together and the result is then added to $\mathbf{e}_{1,m}$. It can be shown that this process requires N and $\frac{3N}{2}$ complex additions for $V = 2$ and $V = 4$, respectively.

TABLE I summarizes the complexity analysis presented above. Figures 6 and 7 show the number of complex mul-

This article has been accepted for publication in a future issue of this journal, but has not been fully edited. Content may change prior to final publication. Citation information: DOI 10.1109/TVT.2015.2395818, IEEE Transactions on Vehicular Technology

TABLE I
COMPUTATIONAL COMPLEXITY COMPARISON OF VARIOUS PAPR REDUCTION SCHEMES

		Number of Complex Multiplications	Number of Complex Additions
Traditional SLM Scheme		$\frac{MN}{2} \cdot \log_2(N)$	$MN \cdot \log_2(N)$
L&W Scheme		$\frac{N}{2} \cdot \log_2(N)$	$N \cdot \log_2(N) + 3MN$
Proposed Scheme	S IFFTs	$\frac{UN}{2} \cdot \log_2(\frac{N}{U \cdot V}) + N \cdot (U-1)$	$UN \cdot \log_2(\frac{N}{U \cdot V})$
	M GCSBs	0	$M \cdot N\left(U - 1 + \frac{V}{4} + \frac{\log_2 V}{2}\right)$

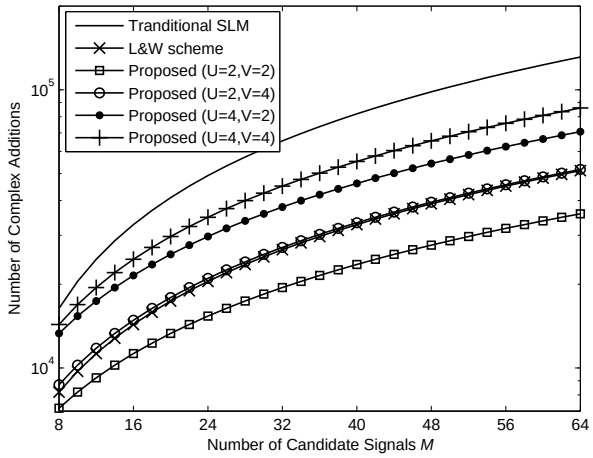

Fig. 7. Number of complex additions as function of number of candidate signals M ($N = 256$).

tiplications and complex additions, respectively, as a function of the number of candidate signals. Note that TABLE I and Figs. 6 and 7 also present results for the traditional SLM method and the method proposed by Li and Wang [15] for comparison purposes. It is seen that the number of complex multiplications in the traditional SLM scheme increases with an increasing number of candidate signals. However, in the proposed scheme and that of Li and Wang, the number of complex multiplications remains constant, irrespective of the number of candidate signals. Of the three schemes, the method proposed in [15] requires the least number of complex multiplications, followed by the scheme proposed in this study with $(U, V) = (2, 4)$ and $(U, V) = (2, 2)$. By contrast, the proposed scheme with $(U, V) = (2, 2)$ requires the minimal number of complex additions, followed by Li and Wang's method and the proposed scheme with $(U, V) = (2, 4)$.

To better illustrate the advantage of the proposed scheme over the traditional SLM scheme, the following computational complexity reduction ratio (CCRR) is introduced:

$$\text{CCRR} = \left\{1 - \frac{\text{Complexity of proposed scheme}}{\text{Complexity of traditional SLM}}\right\} \cdot 100\%. \quad (22)$$

The corresponding results are presented in TABLE II for the case of an OFDM system with $N = 256$. Notably, it is seen that the performance advantage of the proposed scheme increases with an increasing number of candidate signals.

VII. SIMULATION RESULTS

The PAPR reduction performance of the proposed scheme was evaluated by means of numerical simulations. Figure 8 shows the PAPR reduction performance of the proposed scheme for an OFDM system with 256 sub-carriers and the 16-quadrature amplitude modulation (16-QAM) scheme. It can be seen that the PAPR reduction performance of the proposed scheme with $(U, V) = (4, 4)$ is extremely close to that of the traditional SLM method. From a detailed inspection, the performance loss of the proposed scheme relative to that of the traditional SLM method is found to be less than 0.001 dB for $M = 32$, $U = 4$, $V = 4$, and $\Pr(\text{PAPR}(\mathbf{x}) > \gamma) = 10^{-4}$. However, the theoretical analysis results demonstrated in TABLE I have shown that the number of complex multiplications and complex additions required in the proposed scheme for $(U, V) = (4, 4)$ are 8.59% and 68.75%, respectively, of those required in the traditional SLM scheme.

Figure 8 shows that the PAPR reduction performance is essentially the same for both $(U, V) = (2, 4)$ and $(U, V) = (4, 2)$. However, Figs. 6 and 7 have shown that the former case has a higher computational complexity. For both cases, the maximum performance loss of the proposed scheme relative to that of the traditional SLM scheme is around 0.1 dB for $M = 32$, and $\Pr(\text{PAPR}(\mathbf{x}) > \gamma) = 10^{-4}$. Finally, Fig. 8 shows that the proposed scheme has a better PAPR reduction performance than the method proposed in [15], irrespective of the (U, V) combination.

Figure 9 demonstrates the PAPR reduction performance for the cases of $N = 512$ and $N = 1024$. It can be seen that PAPR increases with the number of sub-carriers. However, the PAPR reduction performances of the proposed scheme are able to approach those of the traditional SLM scheme.

This article has been accepted for publication in a future issue of this journal, but has not been fully edited. Content may change prior to final publication. Citation information: DOI 10.1109/TVT.2015.2395818, IEEE Transactions on Vehicular Technology

TABLE II
COMPUTATIONAL COMPLEXITY REDUCTION RATIO OF PROPOSED SCHEME RELATIVE TO TRADITIONAL SLM SCHEME

	$M = 8$			
	$U = 2,\ V = 2$	$U = 2,\ V = 4$	$U = 4,\ V = 2$	$U = 4,\ V = 4$
Multiplications	78.13%	81.25%	59.38%	65.63%
Additions	56.25%	46.88%	18.75%	12.5%
	$M = 16$			
Multiplications	89.07%	90.63%	79.69%	82.81%
Additions	65.63%	54.69%	34.38%	25%
	$M = 32$			
Multiplications	94.53%	95.31%	89.84%	91.41%
Additions	70.31%	58.59%	42.19%	31.25%

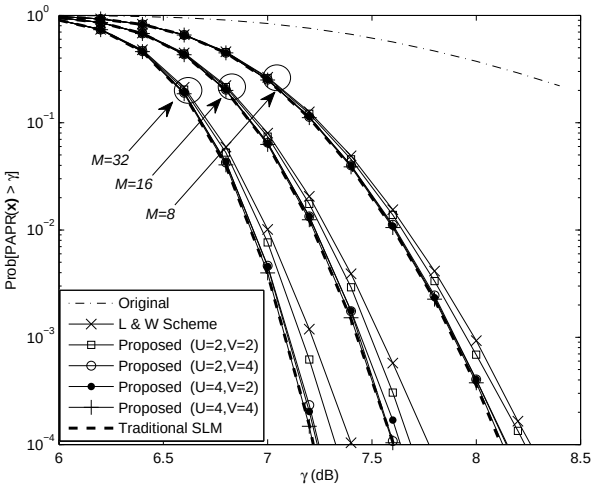

Fig. 8. PAPR reduction performance of various schemes (16-QAM, $N = 256$).

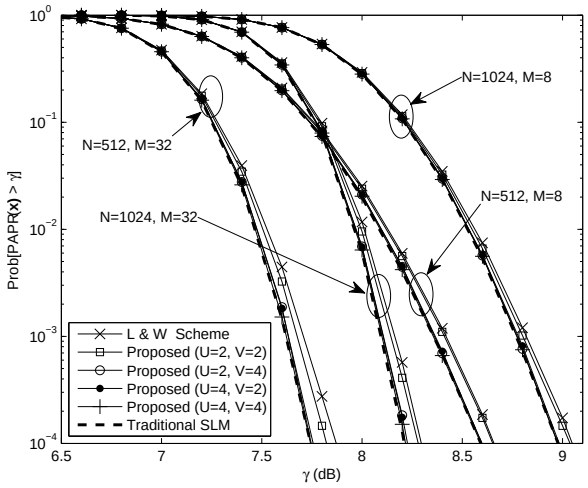

Fig. 9. PAPR reduction performance of various schemes (16-QAM, $N = 512, 1024$).

If U and V are properly selected, the performance loss of the proposed scheme relative to that of the traditional SLM scheme is negligible.

It is worthy of note that the traditional SLM scheme has an arbitrary phase rotation in each sub-carrier and thus has optimal PAPR reduction performance. However, the equivalent frequency-domain phase rotation of each sub-carrier is not arbitrary in our proposed scheme. Subsequently, the equivalent frequency-domain phase rotation is subject to the limited number of phases given in (9), leading to substantial degradation in PAPR reduction performance. Therefore, the proposed scheme increases the equivalent frequency-domain operations (discrete time-domain operations) to maximize the PAPR diversity. However, regardless of the number of discrete time-domain operations performed in our proposed scheme, the PAPR reduction performance can only approach that of the traditional SLM scheme. The difference in our proposed low-complexity scheme is negligible.

A series of simulation experiments are conducted to investigate the PAPR reduction performance when various combinations of frequency-domain operations are performed. The results are demonstrated in Fig. 10, where the PAPR reduction performance basically increases with the number of extra frequency-domain operations. Fig. 10 indicates that the improvement for *Properties 1+2+3* is only marginal compared with *Properties 1+2*. Thus, the contribution of *Property 3* (frequency-domain complex conjugate) is insignificant. However, the PAPR reduction performance when *Properties 1+3* are adopted is better than when *Property 1* alone is adopted. Therefore, the effect of equivalent frequency-domain operation

This article has been accepted for publication in a future issue of this journal, but has not been fully edited. Content may change prior to final publication. Citation information: DOI 10.1109/TVT.2015.2395818, IEEE Transactions on Vehicular Technology

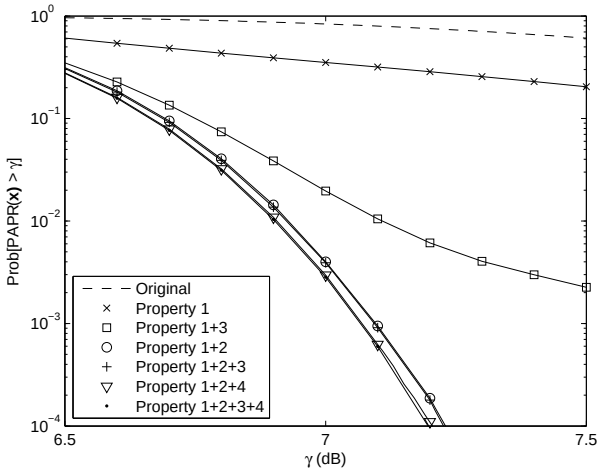

Fig. 10. PAPR reduction performance of various combinations of frequency-domain operations (16-QAM, $M = 32$, $N = 256$, $U = 4$, $V = 4$).

in PAPR reduction depends on their order of operations. In addition, the PAPR reduction performance in general increases with the number of frequency-domain operations. Fig. 10 also illustrates that the PAPR reduction performance of *Properties 1+2+3+4* is better than that of *Properties 1+2+4*, though the improvement is only marginal. The computational complexity of *Properties 1+2+3+4* is the same as that of *Properties 1+2+4*. Thus, all properties should be adopted to obtain the best PAPR reduction performance.

VIII. Conclusions

This paper has presented a new low-complexity architecture for PAPR reduction in OFDM systems. Compared to the traditional SLM scheme, in which the candidate signals are generated using frequency-domain phase rotation only, the architecture proposed in this study additionally uses frequency-domain cyclic shifting, complex conjugate and sub-carrier reversal operations to maximize the PAPR diversity of the candidate signals. In order to avoid the multiple-IFFT problem inherent in the traditional SLM method, the proposed scheme converts all four frequency-domain operations into time-domain equivalent operations. It has been shown that the computational complexity of the proposed approach can be minimized through an appropriate partitioning and reassembling of the sub-carriers in the OFDM system. In addition, the theoretical analysis results have shown that the number of complex multiplications and complex additions required in the proposed scheme for $(U, V) = (4, 4)$ are 8.59% and 68.75%, respectively, of those required in the traditional SLM scheme. Furthermore, the simulation results have shown that the performance loss of the proposed scheme relative to that of the traditional SLM scheme is less than 0.001 dB for 16-QAM, $M = 32$, $N = 256$, $U = 4$, $V = 4$, and $\Pr(\mathrm{PAPR}(\mathbf{x}) > \gamma) = 10^{-4}$. In other words, the proposed scheme closely approximates the PAPR reduction performance of the traditional SLM method, but with a significantly reduced computational complexity.

References

[1] J.-C. Chen and C.-P. Li, "Tone reservation using near-optimal peak reduction tone set selection algorithm for PAPR reduction in OFDM systems," *IEEE Signal Process. Lett.*, vol. 17, no. 11, pp. 933–936, Nov. 2010.

[2] H. Li, T. Jiang, and Y. Zhou, "An improved tone reservation scheme with fast convergence for PAPR reduction in OFDM systems," *IEEE Trans Broadcast.*, vol. 57, no. 4, pp. 902–906, Dec. 2011.

[3] S. Gazor and R. AliHemmati, "Tone reservation for OFDM systems by maximizing signal-to-distortion ratio," *IEEE Trans. Wireless Commun.*, vol. 11, no. 2, pp. 762–770, Feb. 2012.

[4] T. Jiang, W. Xiang, P. C. Richardson, D. Qu, and G. Zhu, "On the nonlinear companding transform for reduction in PAPR of MCM signals," *IEEE Trans. Wireless Commun.*, vol.6, no. 6, pp. 2017–2021, Jun. 2007.

[5] J.-C. Chen and C.-K. Wen, "PAPR reduction of OFDM signals using cross-entropy-based tone injection schemes," *IEEE Signal Process. Lett.*, vol. 17, no. 8, pp. 727–730, Aug. 2010.

[6] B. S. Krongold and D. L. Jones, "PAR reduction in OFDM via active constellation extension," *IEEE Trans. Broadcast.*, vol. 49, no. 3, pp. 258–268, Sep. 2003.

[7] K. Bae, J. G. Andrews, and E. J. Powers, "Adaptive active constellation extension algorithm for peak-to-average ratio reduction in OFDM," *IEEE Commun. Lett.*, vol. 14, no. 1, pp. 39–41, Jan. 2010.

[8] P. Van Eetvelt, G. Wade, and M. Tomlinson, "Peak to average power reduction for OFDM schemes by selective scrambling," *Elect. Lett.*, vol. 32, no. 21, pp. 1963–1964, Oct. 1996.

[9] A. D. S. Jayalath and C. Tellambura, "Reducing the peak-to-average power ratio of orthogonal frequency division multiplexing signal through bit or symbol interleaving," *Electron. Lett.*, vol. 36, no. 13, pp. 1161–1163, Jun. 2000.

[10] L. J. Cimini, Jr. and N. R. Sollenberger, "Peak-to-average power ratio reduction of an OFDM signal using partial transmit sequences," *IEEE Commun. Lett.*, vol. 4, no. 3, pp. 86–88, Mar. 2000.

[11] J.-C. Chen, "Application of quantum-inspired evolutionary algorithm to reduce PAPR of an OFDM signal using partial transmit sequences technique," *IEEE Trans. Broadcast.*, vol. 56, no. 1, pp. 110–113, Mar. 2010.

[12] T. Jiang and C. Li, "Simple alternative multi-sequences for PAPR reduction without side information in SFBC MIMO OFDM systems," *IEEE Trans. Veh. Technol.*, vol. 61, no. 7, pp. 3311–3315, Sep. 2012.

[13] R. W. Baüml, R. F. H. Fisher, and J. B. Huber, "Reducing the peak-to-average power ratio of multicarrier modulation by selected mapping," *Elect. Lett.*, vol. 32, no. 22, pp. 2056–2057, Oct. 1996.

[14] C.-L. Wang and Y. Ouyang, "Low-complexity selected mapping schemes for peak-to-average power ratio reduction in OFDM systems," *IEEE Trans. Signal Process.*, vol. 53, no. 12, pp. 4652–4660, Dec. 2005.

[15] C.-P. Li, S.-H. Wang, and C.-L. Wang, "Novel low-complexity SLM schemes for PAPR reduction in OFDM systems," *IEEE Trans. Signal Process.*, vol. 58, no. 5, pp. 2916–2921, May 2010.

[16] S.-H. Wang, J.-C. Sie, and C.-P. Li, "A low-complexity PAPR reduction scheme for OFDMA uplink systems," *IEEE Trans. Wireless Commun.*, vol. 10, no. 4, pp. 1242–1251, Apr. 2011.

[17] W.-W. Hu, S.-H. Wang, and C.-P. Li, "Gaussian integer sequences with ideal periodic autocorrelation functions," *IEEE Trans. Signal Process.*, vol. 60, no. 11, pp. 6074–6079, Nov. 2012.

[18] S.-H. Wang, K.-C. Lee, C.-P. Li, and H.-J. Li, "A low-complexity symbol interleaving-based PAPR reduction scheme for OFDM systems," in *Proc. IEEE International Conference on Communications (IEEE ICC 2013)*, June 2013.

[19] H. V. Sorensenand and C. S. Burrus, "Efficient computation of the DFT with only a subset of input or output points," *IEEE Trans. Signal Process.*, vol. 41, no. 3, pp. 1184–1200, Mar. 1993.

This article has been accepted for publication in a future issue of this journal, but has not been fully edited. Content may change prior to final publication. Citation information: DOI 10.1109/TVT.2015.2395818, IEEE Transactions on Vehicular Technology

Sen-Hung Wang received the B.S. degree in Electrical Engineering from National Dong Hwa University, Hualien, Taiwan, in 2004, the M.S. degree in Communications Engineering and the Ph.D. degree in Electrical Engineering from National Sun Yat-sen University, Kaohsiung, Taiwan, in 2006 and 2010, respectively. From 2011 to 2014, Dr. Wang was a Postdoctoral Research Fellow with the Intel-NTU Connected Context Computing Center, National Taiwan University, Taipei, Taiwan. He is currently an Assistant Research Fellow with the Institute of Communications Engineering, National Sun Yat-sen University, Kaohsiung, Taiwan. His research interests include wireless communication, signal processing, sequence design, multiple access technology, machine-to-machine communication, and the fifth generation mobile communication technology.

Kuan-Chou Lee received the B.S. degree in Electrical Engineering from the Fu Jen Catholic University, Taipei, Taiwan, in 2007, the M.S. degree in Communications Engineering from National Sun Yat-sen University, Kaohsiung, Taiwan, in 2009 and the Ph.D. degree in Communication Engineering from National Taiwan University, Taipei, Taiwan, in 2014. He currently works in the Mstar semiconductor, Inc. His main research interests include wireless communication, OFDM, cooperative, and signal processing.

Chih-Peng Li received the B.S. degree in Physics from National Tsing Hua University, Hsin Chu, Taiwan, in June 1989 and the Ph.D. degree in Electrical Engineering from Cornell University, Ithaca, NY, USA, in December 1997.

From 1998 to 2000, Dr. Li was a Member of Technical Staff with the Lucent Technologies. From 2001 to 2002, he was a Manager of the Acer Mobile Networks. In 2002, he joined the faculty of the Institute of Communications Engineering, National Sun Yat-sen University, Kaohsiung, Taiwan, as an assistant professor. He has been promoted to Professor in 2010. Dr. Li is currently the Chairman of the Department of Electrical Engineering and the Director of the International Masters Program in Electric Power Engineering. His research interests include wireless communications, baseband signal processing, and data networks.

Dr. Li is currently the Chair of the IEEE Communications Society Tainan Chapter, the Chair of the IEEE Broadcasting Technology Society Tainan Chapter, the Vice Chair of Chapter Coordination Committee for IEEE Asia Pacific Board, and the President of Taiwan Institute of Electrical and Electronics Engineering (TIEEE). Dr. Li also serves as the Editor of the IEEE Transactions on Wireless Communications, the Associate Editor of the IEEE Transactions on Broadcasting, and the General Chair of 2014 IEEE Vehicular Technology Society Asia Pacific Wireless Communications Symposium (IEEE VTS APWCS 2014). Dr. Li was the lead guest editor of the Special Issue on Advances in Antenna Design and System Technologies for Next Generation Cellular Systems, International Journal of Antennas and Propagation. He was also the recipient of the 2014 Outstanding Professor Award of the Chinese Institute of Electrical Engineering Kaohsiung Branch.